

pubs.acs.org/acscatalysis Research Article

# First-Principles Analysis of Ethylene Oligomerization on Single-Site Ga<sup>3+</sup> Catalysts Supported on Amorphous Silica

Yinan Xu, Nicole J. LiBretto, Guanghui Zhang, Jeffrey T. Miller, and Jeffrey Greeley\*



Cite This: ACS Catal. 2022, 12, 5416-5424



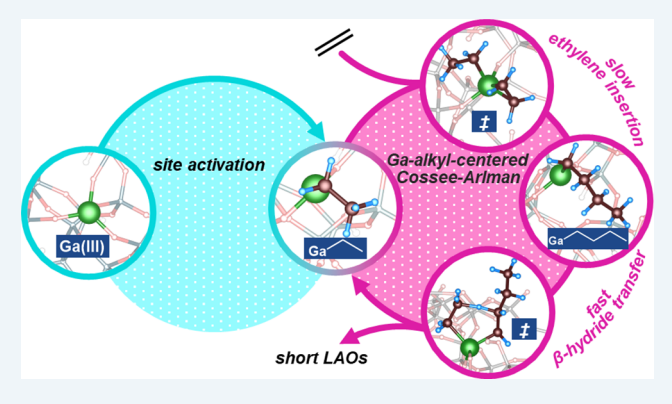
**ACCESS** 

Metrics & More



s Supporting Information

ABSTRACT: Amorphous, single-site, silica-supported main group metal catalysts have recently been found to promote olefin oligomerization with high activity at moderate temperatures and pressures (~250 °C and 1 atm). Herein, we explore the molecular level relationship between active site structures and the associated oligomerization mechanisms by developing amorphous, silica-supported Ga³+ models from periodic, first principles calculations. Representative Ga³+ sites, including three- and four-coordinated geometries, are tested for multiple ethylene oligomerization pathways. We show that the three-coordinated Ga³+ site promotes oligomerization through a facile initiation process that generates a Ga-alkyl intermediate, followed by a Ga-alkyl-centered Cossee—Arlman mechanism. The strained geometry of the three-coordinated site enables a favorable free-energy landscape with a



kinetically accessible ethylene insertion transition state (1.7 eV) and a previously unreported  $\beta$ -hydride transfer step (1.0 eV) to terminate further C–C bond formation. This result, in turn, suggests that  $Ga^{3+}$  does not favor polymerization chemistry, while microkinetic modeling confirms that ethylene insertion is the rate-determining step. The study demonstrates the promising flexibility of the main group ions for hydrocarbon transformations and, more generally, highlights the importance of the local geometry of metal ions on amorphous oxides in determining catalytic properties.

KEYWORDS: heterogeneous catalysis, amorphous silica, single site, olefin oligomerization, reaction pathways, main group chemistry

#### ■ INTRODUCTION

Light olefins (ethylene and propylene) are the fundamental building blocks of the petrochemical industry. The molecules are readily available and can be converted to a wide range of useful intermediate and final products. 1-3 The production of short linear alpha olefins (LAOs), in particular, has been of significant interest in the olefin industry for the past few decades, as these chemicals form the key ingredients of various plastics, lubricants, fuels, and surfactants. 4,5 Production of LAOs, such as 1-butene, 1-hexene, and 1-octene, through selective catalytic olefin oligomerization has, in turn, become a core research topic in the olefin community due to both the existence of many emerging alternative sources of light olefins and the increasing demand for polyethylene. 5-7 Presently, homogeneous catalysts, using ligand-modified transition metals, are among the most active and selective catalysts for olefin oligomerization.<sup>8–10</sup> Among the transition metals, nickel complexes are commonly used, where the Ni2+ compounds modified with alkyl or hydride moieties are the active catalytic centers. 10-13 Many efforts have also been devoted to developing heterogeneous catalysts for oligomerization, given their greater ability for catalyst regeneration and product separation. As an example, reactive transition-metal species,

inspired by analogous structures on homogeneous catalysts, can be supported on porous structures, such as zeolites and amorphous silica, but these catalysts suffer from poor oligomerization activity or low selectivity to LAOs. 14–19

Density functional theory (DFT)-based studies are becoming increasingly important in elucidating the structures and properties of active sites, as well as the reaction mechanisms, of heterogeneously catalyzed olefin oligomerization processes such as those discussed above. <sup>20–25</sup> For instance, a recent first-principles study by Brogaard et al. investigated Ni(0), Ni<sup>+</sup>, and Ni<sup>2+</sup> supported on an SSZ-24 framework in the context of ethylene oligomerization. The work revealed that the most plausible pathway starts from a [Ni(II)-ethylene-H]<sup>+</sup> complex, analogous to a Ni-alkyl ligand in the homogeneous context, and the oligomerization chemistry follows the classic Cossee—Arlman (CA) mechanism, where ethylene coordinates and

Received: December 23, 2021 Revised: April 1, 2022 Published: April 21, 2022





ACS Catalysis pubs.acs.org/acscatalysis Research Article

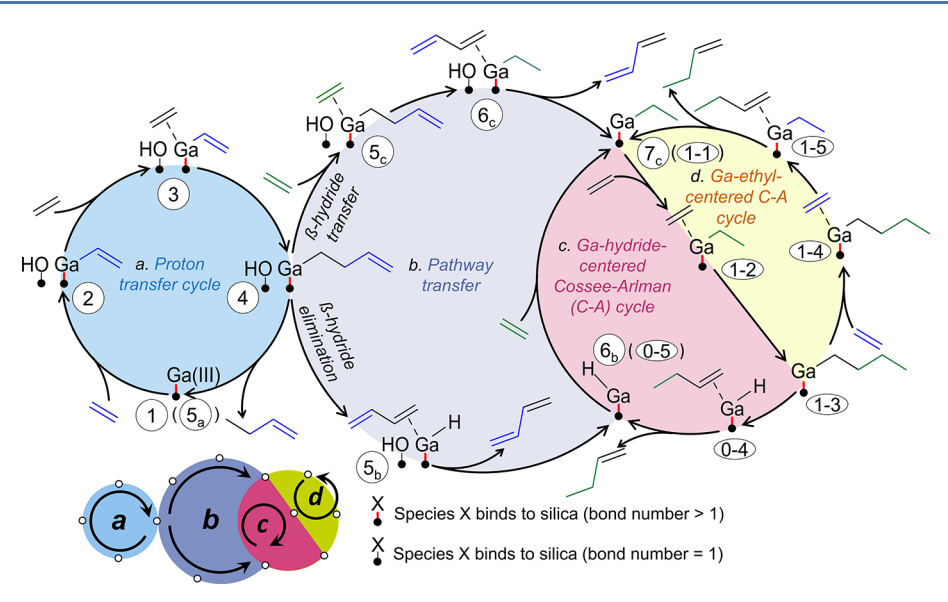


**Figure 1.** Possible ethylene oligomerization pathways on amorphous silica-supported Ga<sup>3+</sup>. A proton transfer cycle begins on empty Ga<sup>3+</sup> sites (region "a"); alternatively, the formation of Ga-hydride or Ga-alkyl species leads to pathway transfer (region "b") to the CA mechanism for ethylene oligomerization, where the CA cycles occur on either Ga-hydride (region "c") or Ga-alkyl sites (region "d"). The corresponding energies and geometries are shown in Figures 3–5.

inserts between the species and the Ni ion, resulting in chain growth. The process is terminated via an ethylene-assisted  $\beta$ -hydride elimination step that restores the [Ni(II)-ethylene-H]<sup>+</sup> moiety. In another mechanistic study by Metzger et al., investigating Ni-MFU-4l for ethylene dimerization, a combination of isotope tracing, molecular probes, and DFT calculations was used to demonstrate that the catalytic cycle also follows the CA mechanism, where ethylene insertion and  $\beta$ -hydride elimination are the key elementary steps.  $^{26}$ 

To expand the space of possible heterogeneous catalysts for olefin oligomerization, single-site, silica-supported main group Ga ions have recently been explored and found to catalyze ethylene and propylene oligomerization to higher molecular weight linear olefins with high selectivity to C<sub>4</sub> oligomers (76%) at 250 °C and atmospheric pressure.<sup>27</sup> Through a combination of in situ and ex situ X-ray absorption spectroscopy (XAS), H/D exchange, IR techniques, and DFT calculations, it was determined that Ga<sup>3+</sup> sites catalyze the oligomerization reaction. The mechanism starts from a site activation process, where a Ga<sup>3+</sup>-O bond is activated, resulting in Ga-vinyl and Si-OH moieties (species 1 and 2, Figure 1). After the activation step, ethylene insertion and  $\beta$ -hydride elimination occur, leading to butadiene and a Ga-hydride site (species  $6_h$ , Figure 1). The Ga-hydride moiety was proposed to be responsible for the subsequent oligomerization cycle, following a CA mechanism (cycle "c", Figure 1).<sup>27</sup>

To further elucidate the mechanistic and structural aspects of oligomerization on silica-based Ga catalysts, it is of interest to explore whether additional factors, such as the intrinsic heterogeneity of amorphous silica, can accommodate the activation of other oligomerization pathways. It is well known that many heterogeneous catalytic reactions on oxide-supported metal ions are highly sensitive to the structure of active sites. <sup>28–31</sup> The Cr<sup>3+</sup>-silica geometry in the Philips catalyst for ethylene polymerization is a useful example, wherein the reactivity of different Cr sites in terms of initiation, propagation, and termination energetics varies significantly with the local strain conditions, causing a small percentage of

the Cr sites to dominate the polymerization chemistry. <sup>29,31</sup> Further, in recent works, an alternate CA cycle with alkene-assisted  $\beta$ -hydride transfer has been explored on both Ni, for oligomerization, <sup>20,22</sup> and Cr, for polymerization, <sup>31,32</sup> and favorable energy landscapes have been observed. Similar considerations may apply to the Ga<sup>3+</sup>-silica system, underlining the need to further explore the link between oligomerization pathway selectivity and the structural diversity of the Ga<sup>3+</sup> single sites.

Herein, we develop amorphous silica-supported Ga<sup>3+</sup> models based on periodic DFT calculations to study ethylene oligomerization mechanisms for the previously synthesized Ga/SiO<sub>2</sub> catalysts. In modeling amorphous silica as the support for Ga3+ single sites, a realistic representation of the amorphous structure is clearly crucial. In the literature, many useful models of amorphous silica have been developed based on SiO<sub>2</sub> clusters. Such cluster models are computationally efficient and permit the simulation of local effects of a catalytic site using high levels of theory. 30,32-34 However, periodic models with appropriately sized unit cells have the advantage of permitting the direct treatment of surface structural inhomogeneity, where silanols and siloxane bridges of various sizes can be accommodated within a single structure.<sup>35</sup> Indeed, in the past 15 years, multiple DFT-based periodic models of amorphous silica have been developed, stemming primarily from the works of Ugliengo, <sup>36</sup> Tielens, <sup>37</sup>, <sup>38</sup> and colleagues. For instance, in the periodic silica model proposed by Ugliengo, the amorphous structure is introduced through an annealing process of bulk cristobalite using classical molecular dynamics, from which a silica slab is extracted and on which dangling oxygen bonds are passivated by hydrogen atoms. Subsequently, slab structures that varied in the degree of hydroxylation were generated through the condensation of adjacent silanol pairs.<sup>36</sup> The fidelity of such amorphous models has been determined by matching the computational and experimental vibrational signatures of silanol moieties.<sup>39</sup> More recently, Comas-Vives and colleagues employed a similar approach and generated an amorphous silica model with a larger unit cell (21.4  $\times$  21.4  $\times$ 

14.2 Å, with a vacuum thickness of 20 Å) containing 402 atoms. 40 In the process of developing silica surfaces with different silanol densities (1.1-7.2 nm<sup>-2</sup>), the authors considered silica migration steps that lead to favorable dehydroxylation energetics, and the dependency of the degree of dehydroxylation on the temperature and partial pressure of water was also explored. 40 In addition to these pioneering contributions, we readily acknowledge the suitability and strengths of other periodic DFT-based treatments of amorphous silica that have been used to model heterogeneous catalytic reactions on metal single sites for a variety of chemistries. <sup>41–45</sup> In particular, we note that Deraet et al. have recently investigated the interactions between transition-metal single sites and silica surfaces using a hydroxylated amorphous model. The authors established that these interactions originate primarily from van der Waals effects (for Ag and Au ions), metal oxophilicity (for Fe, Co, and Ni ions), and from electron transfer effects (for Ru, Os, Ir, and Pt ions).46

In this work, we adapt the Comas-Vives model of amorphous silica to create a variety of Ga<sup>3+</sup> sites for subsequent catalytic analysis (Figure 2). On this surface, the

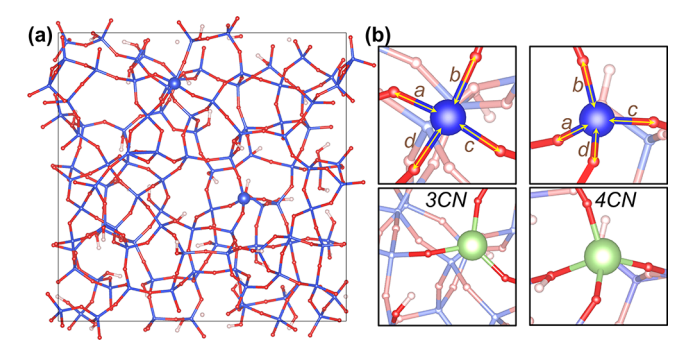


**Figure 2.** (a) Top view of the unit cell of the amorphous silica model, with locations of the Si atoms used for creating 3CN and 4CN sites and (b) bonding conditions of the original Si atoms and the corresponding Ga sites after DFT optimization (Ga = green, O = red, Si = blue, and H = white).

energetics of three primary cycles of ethylene oligomerization are compared, as shown in Figure 1. A proton transfer cycle can occur on the empty Ga<sup>3+</sup> sites, starting from ethylene activation by Ga3+, followed by the insertion of another ethylene unit (species 1 to 4, Figure 1). The resulting Gabutenyl species can then desorb via a proton transfer step, forming *n*-butene and completing the oligomerization cycle via proton transfer and reforming the empty Ga<sup>3+</sup> site (region "a", Figure 1).<sup>47</sup> Alternatively, the Ga-butenyl species may activate pathway transfer processes (region "b", Figure 1).  $\beta$ -hydride elimination can then activate another oligomerization cycle, where butadiene and Ga-hydride are formed, proceeding to a CA mechanism (species  $4-6_b$ , Figure 1). Further, as mentioned above,  $\beta$ -hydride elimination can be assisted by an incoming alkene molecule, which accepts a hydrogen atom and becomes an alkyl intermediate, which may, in turn, constitute another key intermediate in the CA cycle (species  $4-7_{c}$ , Figure 1). Following the pathway transfer process, the CA cycle can be either Ga-hydride-centered (region "c", Figure 1) or Ga-alkyl-centered (region "d", Figure 1), and the two cycles differ by terminating the oligomer chain growth through  $\beta$ -hydride elimination or by directly transferring hydrogen to an ethylene molecule. In our Ga/SiO2 system, we report that only the less-constrained, three-coordinated  $Ga^{3+}$  site is responsible for the oligomerization reactivity through the Gaalkyl-centered CA cycle, for which the free energy landscape is significantly more favorable than the competing proton transfer and the hydride-centered CA mechanisms. The selective ethylene dimerization observed in experiments is enabled by a previously unreported transition state of the ethylene-assisted  $\beta$ -hydride transfer step to terminate the lengthening of the carbon backbone for which the activation energy is much lower than that of the ethylene insertion step. Finally, a detailed microkinetic analysis is carried out, based on the DFT results, which establishes that the ethylene insertion step is rate-limiting. In aggregate, these insights establish a comprehensive mechanistic understanding of how amorphous silica-supported main group single sites catalyze olefin oligomerization.

#### METHODS

Single-site Ga<sup>3+</sup>-silica structures are developed, as described in the literature (see Introduction for a detailed description), starting from an amorphous silica slab model created through an annealing procedure using molecular dynamics and continuous dehydroxylation processes.<sup>40</sup> The periodic model has a sufficiently large unit cell to incorporate the possibility of long-range reconstructions and interactions (Figure 2). A highly dehydroxylated surface with a low silanol density is chosen (1.1 nm<sup>-1</sup>) due to the high temperature used in catalyst synthesis in experiments  $(T_{\text{calcination}} = 823 \text{ K}).^{27}$  The silica unit cell contains five isolated silanol groups, where the shortest distance between each silanol pair is 5.8 Å. Additional geometric details are provided in the Supporting Information (S.1). The high degree of structural inhomogeneity in the amorphous silica model is reflected in the high variability in the dehydroxylation energy  $(1-322 \text{ kJ mol}^{-1})$ , as well as the Si-O bond lengths of the newly created siloxane rings (1.65-1.75 Å), as reported in the work by Comas-Vives. 40 To create each single-atom Ga3+ site, a Si atom in the amorphous model is replaced with Ga, and a proton is added to an adjacent oxygen atom to maintain charge balance.

The calculations are based on self-consistent, periodic density functional theory using the Vienna Ab-initio Simulation ackage (VASP). The BEEF-VdW exchange-correlation functional<sup>51</sup> with projector-augmented wave (PAW) pseudopotentials is employed. 52 A dipole layer is applied in a vacuum to eliminate the electrostatic interaction errors between mirror image slabs. A k-point grid of  $2 \times 2 \times 1$ is used based on the Monkhorst-Pack k-sampling, and the convergence of the binding energy with respect to the k-point set is confirmed. A cutoff energy of 400 eV and a force convergence criterion of 20 meV Å<sup>-1</sup> for local energy minimization are used. The climbing image nudged elastic band (CINEB) method, with seven intermediate images, is used to locate the geometry of transition states, 53,54 with initial guesses generated using the image-dependent pair potential tool.<sup>55</sup> After the CINEB calculations converge to a force below 80 meV  $\text{Å}^{-1}$  for each image, the Lanczos diagonalization approach is employed to refine the transition state. 56 The force convergence criterion of the Lanczos optimization is 40 meV

Free energies are evaluated at 523 K and are calculated using the equation  $G = E_{\rm DFT} + E_{\rm ZPE} - TS$ , where  $E_{\rm DFT}$  is the ground state potential energy from DFT. The zero-point energy corrections ( $E_{\rm ZPE}$ ) are calculated from the harmonic vibrational states. In the analysis of vibrational modes, atoms belonging to

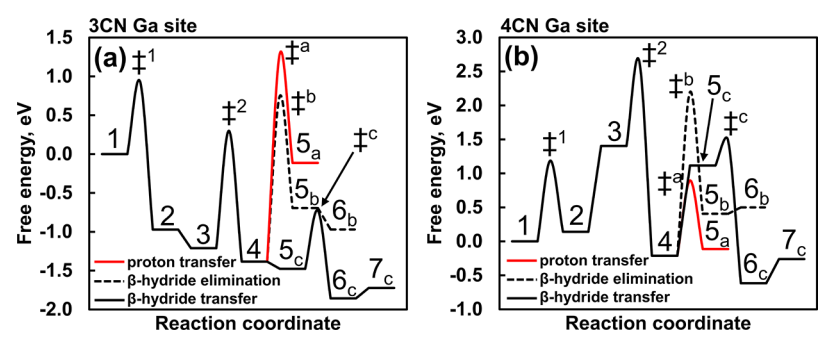


Figure 3. Free energy diagrams of proton transfer and pathway transfer processes (through β-hydride elimination and ethylene-assisted β-hydride transfer) on (a) 3CN and (b) 4CN Ga sites (T = 523 K). The pathway transfer processes involve site activation, leading to Ga-hydride or Ga-ethyl species. The adsorption energies are referenced to the empty sites and appropriate amounts of gaseous ethylene molecules at 1 atm. The overall reaction energy changes differ between the 3CN and 4CN sites because the transition from species 1 to  $7_c$  corresponds to site opening and is not, therefore, a closed catalytic cycle. The same species numbers are used as in Figure 1.

the adsorbate, the Ga site, and nearest-neighbor oxygen atoms on the silica surface are allowed to move. For vibrational modes with wavenumbers above 150 cm<sup>-1</sup>, harmonic partition functions are employed to estimate entropies. For modes with lower frequencies, particle-in-a-box (PIB) and free rotor schemes, depending on the geometric characteristics of the vibrations, are used (see, e.g., Supporting Information S.9). The adsorption energies  $(G_{ads})$  are referenced to the empty sites (G<sub>Ga</sub>) and appropriate amounts of gaseous ethylene molecules at 1 atm ( $G_{\text{ethylene}}$ ). However, the free energy of Gahydride or Ga-alkyl moieties is used for the  $G_{Ga}$  term in the CA cycles. The gas phase reaction energy of ethylene dimerization is calculated from DFT and is compared to experimental data from NIST. Based on this comparison, a correction of -0.09eV is applied to the calculated gas phase energy of 1-butene (see additional details in Supporting Information S.4).

The microkinetic model simulates a continuously stirred tank reactor (CSTR) with no concentration or temperature gradients. The reaction conditions used in the model are configured to be close to those in our experimental setup.<sup>2</sup> Ethylene oligomerization is modeled at a temperature of 523 K and a total pressure of 1 atm. The reactor has dimensions of 1 cm  $\times$  1 cm  $\times$  1 cm, the feed stream contains 20% of ethylene and 80% inert gas unless otherwise stated, and the feed volumetric flow rate is 1 cm<sup>3</sup> s<sup>-1</sup>. The total number of available Ga sites is used to adjust the conversion of ethylene. Here, a base value of  $0.6 \times 10^{-5}$  mol of Ga sites per gram of catalyst is used, corresponding to a small catalyst loading (0.04 wt %). We use this value because a Ga loading of 3 wt % was used in the experiments in the previous work, and we assume that approximately 1% of the total Ga sites are reactive. <sup>27</sup> Finally, a degree of rate control (DRC) analysis is performed to identify the rate-determining steps.<sup>57</sup> We perform this analysis by introducing differential changes of the individual activation barrier, followed by the determination of how the reaction rate varies in response to these changes. Additional information concerning the microkinetic model and the DRC analysis is found in the Supporting Information (S.8).

#### RESULTS AND DISCUSSION

**Ga Site Creation.** As discussed in the Methods section, each single-site Ga<sup>3+</sup> ion in an amorphous silica model is introduced by a substitution technique, resulting in a Si–OH moiety. In total, five Si atoms, as shown in Figure S1, are considered and substituted individually. As a Si atom binds to four O atoms, there are four possible locations where a proton

can be added. Therefore, a total of 20 DFT optimizations are performed to develop the Ga site structures for ethylene oligomerization on  $Ga/SiO_2$ .

As different Ga sites are created, the resulting oxygen atom of the Si-OH group can be either distant from, or close to, Ga. The possible extremes in the active site structure are, in turn, represented by two Ga sites with substantially different Ga-Si-OH distances, and these are used as illustrative cases in the analysis that follows. In one case, the original Si-O bonds are elongated (Figure 2b: a = 1.80 Å, b = 1.66 Å, c = 1.76 Å, and d= 1.69 Å). As a result, the addition of hydrogen to the oxygen atom, leading to the cleavage of the bond (a), gives a final Ga-O distance of 4.57 Å after DFT optimization. In the second case, the Si atom used for creating the Ga site is located in a much more constrained framework, reflected by the shorter Si-O bonds (a = 1.66 Å, b = 1.62 Å, c = 1.67 Å, and d = 1.64 ÅÅ). As a result, the newly formed Si-OH group gives a Ga-O bond length of 2.02 Å. In the first of these cases, the Ga atom covalently binds to three oxygen atoms, which makes the Ga site three-coordinated. In the second case, the additional, short, Ga-Si-OH bond is considered as another coordination. Hence, the two extremes are defined as the three- and fourcoordinated Ga sites (3CN and 4CN).

A complete list of the Ga-hydroxyl distances of the 20 tested sites is included in Table S1. We emphasize that the 3CN and 4CN sites, described above, approximately bound the range of the calculated Ga-hydroxyl distances in the various considered configurations. As such, we note that the amorphous silica model is particularly useful in that it can accommodate both stretched and constrained Si-O bonds, thus permitting the analysis of a wide spectrum of coordination conditions of the Ga sites. We further note that, in our experimental results, XAS on Ga/SiO2 indicates that the majority of sites are Ga<sup>3+</sup> with four Ga-O bonds, consistent with the 4CN site model. However, because XAS is a bulk technique, the possible formation of a small amount of 3CN Ga<sup>3+</sup> sites (<10%) cannot be excluded, <sup>27</sup> and exploration of the catalytic relevance of these possible minority sites on amorphous silica is a further motivation for the inclusion of the 3CN Ga sites in our analysis.

Ga<sup>3+</sup> Site Activation Process on 3CN Sites. The free energy diagrams of three pathways on the 3CN Ga site, evaluated at 523 K, are shown in Figure 3, including both the proton transfer mechanism (species  $1-5_a$  in Figure 1) and two pathway transfer processes that form either Ga-hydride (species  $6_b$ ) or Ga-alkyl (species  $7_c$ ) intermediates. The proton

transfer step closes an oligomerization cycle and reforms the empty Ga site (region "a", Figure 1). The Ga-hydride and Gaethyl moieties are, in turn, key intermediates in the CA oligomerization mechanism (regions "c" and "d", Figure 1).

Starting from the empty Ga site (species 1 in Figure 4a), a C–H bond in ethylene is heterolytically cleaved, producing a

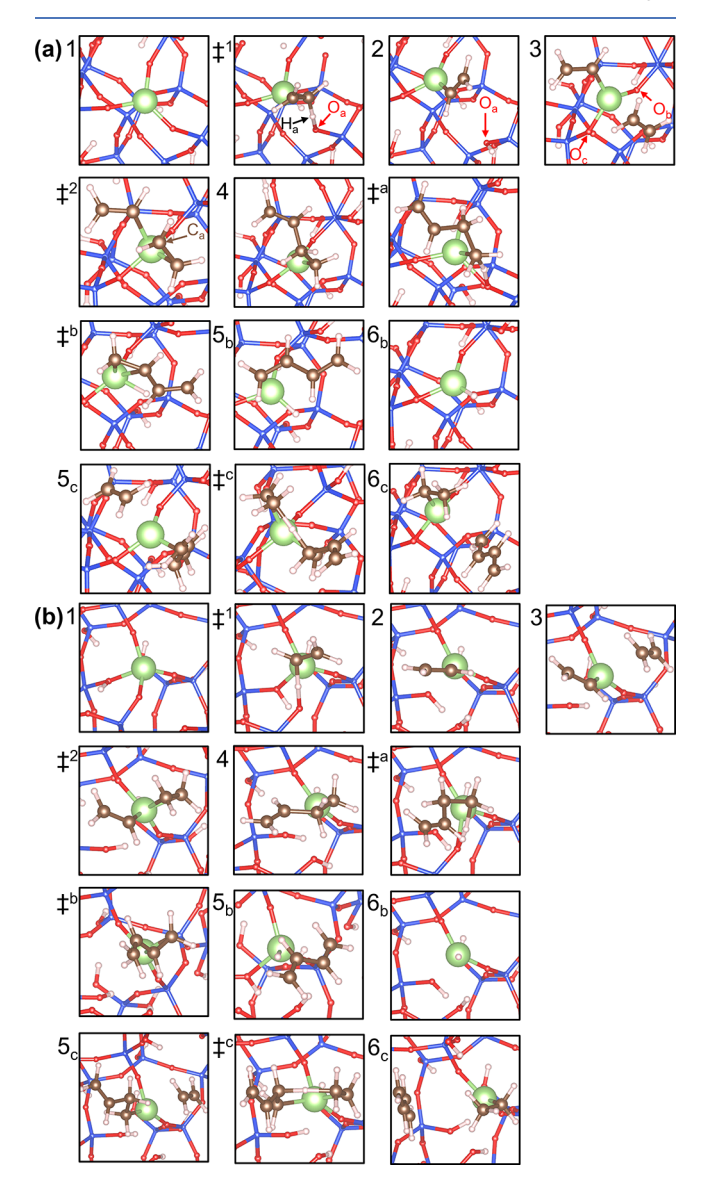


Figure 4. Schematics of proton transfer and pathway transfer on the (a) 3CN site and (b) 4CN Ga sites (Ga = green, O = red, Si = blue C = black, and H = white. The same species numbers are used as in Figure 1).

vinyl group, and the resulting proton  $(H_a)$  from the cleavage associates with an oxygen atom  $(O_a)$  and breaks the Ga–O bond. The newly formed Si–OH group becomes distant from the Ga site, with a Ga–O bond length of 4.2 Å. The heterolytic cleavage is exothermic, with a free energy change of -1.0 eV and an activation energy of 0.9 eV (step 1 to 2). Before the subsequent ethylene insertion occurs, a local energy minimum is found where ethylene is physisorbed on the Ga site (species 3). The C=C double bond coordinates to the planar, triangular geometry created by the Ga atom and two adjacent oxygen atoms (denoted " $O_b$ " and " $O_c$ "). The physisorption is exothermic on the 3CN site (step 2 to 3, -0.2 eV), after which

the migratory insertion of another ethylene molecule leads to a Ga-butenyl species with an activation barrier of 1.5 eV (step 3 to  $\ddagger^2$ ). In the transition state (species  $\ddagger^2$ ), the vinyl group rotates slightly toward the ethylene molecule and interacts with both Ga and a carbon atom (denoted "C<sub>a</sub>" in the figure), which eventually becomes the  $\beta$ -carbon of the Ga-butenyl species.

Pathway Transfer on the 3CN Site. As the  $C_4$ intermediate forms, ethylene-assisted  $\beta$ -hydride transfer is the most favorable pathway due to a generally lower free energy landscape (species  $4-7_{\circ}$  Figure 3a). In this pathway, the physisorption of a third ethylene moiety is slightly exothermic (step 4 to  $5_{\circ}$  –0.1 eV), and the activation barrier of  $\beta$ -hydride transfer is 0.8 eV (step 5, to ‡c). Overall, the free energy of forming a Ga-ethyl intermediate from a clean 3CN Ga (species 1 in Figure 4a) site is -1.7 eV, and the Ga-ethyl species is thus quite likely to form. In contrast to this  $\beta$ -hydride transfer step, high barriers are observed for both the proton transfer and the  $\beta$ -hydride elimination steps. Indeed, the proton transfer step entails the recovery of the cleaved Ga-O bond, which is quite high in energy due to the strained nature of the 3CN site. We note, in passing, that similar high activation barriers for  $\beta$ hydride elimination have also been observed for Zn-propyl species during propane dehydrogenation.<sup>58</sup>

Proton Transfer Cycle Compared to Pathway Transfer Processes on the 4CN Site. The free energy diagrams (523 K) of proton transfer (species  $1-5_a$ , Figure 1),  $\beta$ -hydride elimination (species 4– $6_b$ ), and ethylene-assisted  $\beta$ -hydride transfer (species 4-7<sub>c</sub>) pathways on the 4CN Ga site are shown in Figure 3b. The 4CN Ga site clearly has a different free energy landscape for site activation than does the 3CN site. Before the migratory insertion of ethylene, the physisorption step is greatly endothermic (step 2 to 3, +1.2 eV), which can be explained by a strong steric hindrance due to the nearby siloxane framework. Although a lower intrinsic activation barrier of ethylene insertion is found (step 3 to ‡<sup>2</sup>, +1.2 eV), the transition state is high in free energy if Ga-vinyl is used as a reference (3CN: 1.2 eV, 4CN: 2.5 eV). Similarly, the positive free energy change of ethylene physisorption leads to a significant energy penalty for ethylene-assisted  $\beta$ -hydride transfer (step 4 to  $5_c$ , +1.3 eV), which is, in contrast, a viable pathway on the 3CN Ga site. As 4CN Ga is in a more constrained environment, the Si-OH group formed due to ethylene activation is not far from the Ga site (2.7 Å in species 4), allowing for a relatively facile proton transfer step to recover the original 4CN Ga site with an accessible activation barrier (step 4 to ‡a, 1.1 eV). Therefore, the 4CN site is more likely to catalyze olefin oligomerization through the proton transfer cycle, though a fairly low turnover frequency is expected due to the high barrier of olefin insertion. On the other hand, a pathway transfer to CA mechanism is very likely to occur on the 3CN Ga site, forming a Ga-alkyl intermediate.

Olefin Oligomerization Following the CA Mechanism on 3CN Sites. In the Ga site activation analysis on 3CN sites, the formation of a Ga-alkyl moiety through  $\beta$ -hydride transfer is the most energetically favorable pathway. Following the site activation, the coordination of an ethylene molecule to the alkyl group occurs, which initiates the CA oligomerization cycle. Our analysis starts from the Ga-alkyl species, and Figure 5a shows the free energy diagram of the CA mechanism on a 3CN site. However, we analyze two types of CA mechanisms (Figure 1), starting from either Ga-hydride or Ga-alkyl. These configurations may, in principle, interconvert. We further analyze the related possibility that 3CN and 4CN sites may

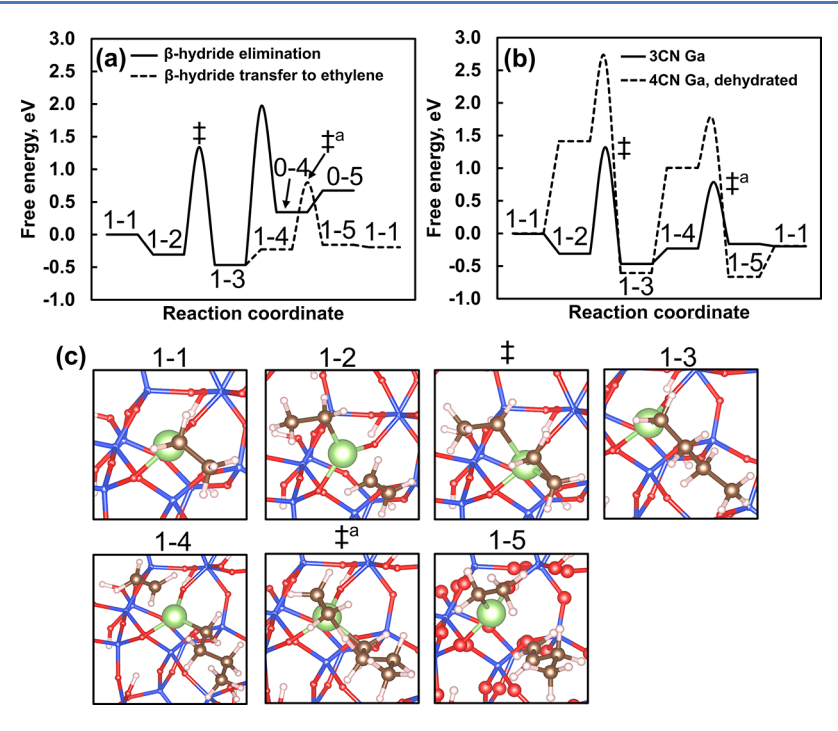


Figure 5. (a) Free energy diagrams of ethylene oligomerization with β-hydride elimination compared to β-hydride transfer pathways on 3CN Ga sites (T = 523 K), (b) free energy diagrams of ethylene oligomerization on 3CN and 4CN sites (dehydrated), and (c) schematics of ethylene oligomerization intermediates on a 3CN site (T = 523 K). The adsorption energies are referenced to Ga-ethyl species and appropriate amounts of gaseous ethylene molecules at 1 atm. The same species numbers are used as in Figure 1.

catalyze the CA mechanism beginning with the Ga-hydride species, which can be produced with a hydrogen gas treatment.<sup>27</sup>

The ethylene physisorption on Ga-ethyl species is exothermic, with a free energy change of -0.3 eV (species 1-1 to 1-2, Figure 5). The migratory insertion of the second ethylene molecule, which approaches Ga and binds to the ethyl group, has an activation barrier of 1.7 eV (species 1-2 to 1-3). Following the physisorption of an additional ethylene molecule, the activation barrier of the  $\beta$ -hydride transfer step (species 1-4 to 1-5, 1.0 eV) is much lower than that of the ethylene insertion step. The  $\beta$ -hydride transfer step finishes one catalytic cycle and reforms the Ga-alkyl species. We have also calculated the barrier of  $\beta$ -hydride elimination leading to the Ga-hydride moiety, for which the barrier is significantly higher than is the ethylene-assisted barrier (species 1-3 to  $\ddagger^b$ , 2.4 eV), suggesting that Ga-hydride is unlikely to form. Overall, based on the free energy analysis, we predict that Gaalkyl favors the formation of short oligomers, as the termination step ( $\beta$ -hydride transfer) will be faster than the propagation step (migratory insertion) due to a much lower activation barrier. This behavior has been observed in the experiments, where butenes are the primary products detected. On the other hand, the CA mechanism will not be dominated by the Ga-hydride species, given the high barrier of the  $\beta$ hydride elimination step.

We note that the transition state geometry of  $\beta$ -hydride transfer on the 3CN Ga site is fundamentally different from the step occurring on a transition metal single site. In the transition states on Ni<sup>2+</sup> or Cr<sup>3+</sup> single sites, the hydrogen atom being transferred is close to the metal center, and this interaction contributes to the stabilization of the transition state. <sup>22,32</sup> In the transition state on a 3CN Ga site (‡a), however, the hydrogen atom being transferred does not interact closely with

the Ga atom, suggesting that Ga does not directly activate the C–H bond. Nevertheless, a low barrier is observed. This geometry was reported for early transition metal-based Ziegler–Natta catalysts, with the associated low barrier being attributed to the pseudo-hydrogen bond effect. <sup>59,60</sup> Our results suggest that a similar effect may extend to main group single sites such as Ga.

Olefin Oligomerization Following the CA Mechanism on a 4CN Site. The activation of ethylene on a 4CN Ga site generates a Si–OH group close to Ga. However, a second Si–OH group is also present due to the original Ga site creation process (species 2 in Figure 4b). The close proximity of the two Si–OH groups leads to the possibility of a dehydration step which gives an oxygen-bridged Si pair and a water molecule. The free energy of dehydration is reasonably negative when water is present at low pressures ( $P_{\text{water}} = 10^{-9}$  atm; see the Supporting Information S.3). Such a step can occur as soon as ethylene is activated, and as the two Si–OH groups are removed, the proton transfer pathway, reforming the original 4CN Ga site, would no longer be viable. As with the Ga site, β-hydride transfer to ethylene would then lead to the CA mechanism dominated by a Ga-ethyl species.

Figure 5b shows the energetics of the CA oligomerization cycle on the 3CN and 4CN Ga sites with a dehydration step. The 3CN site generally exhibits a much more favorable energy landscape. Specifically, low activation barriers of both ethylene migratory insertion (3CN: 1.7 eV) and  $\beta$ -hydride transfer (3CN: 1.0 eV) are observed. On the 4CN dehydrated site, the ethylene physisorption steps before insertion and  $\beta$ -hydride transfer show positive changes in free energies (1.4 and 1.6 eV, respectively), leading to significantly higher overall barriers of ethylene insertion.

Olefin Oligomerization Following the Ga-Hydride-Centered CA Mechanism. As mentioned above, the CA mechanism could potentially be Ga-hydride-centered (region "c", Figure 1), and these sites could be produced through a hydrogen gas treatment.<sup>27</sup> To explore this possibility, we have analyzed the free energy landscapes of the Ga-hydride-centered CA mechanism on both 3CN and 4CN sites (Figures S5-S7). High activation barriers are involved in the  $\beta$ -hydride elimination steps (4CN: 2.5 eV, 3CN: 2.3 eV), while the alternative  $\beta$ -hydride transfer step, producing Ga-ethyl species, exhibits much lower activation barriers. Further, high activation barriers of ethylene insertion are consistently observed for the 4CN sites (2.9 eV). Therefore, we conclude that the Ga-ethyl-centered CA mechanism is the most favorable pathway on the Ga/SiO<sub>2</sub> system, and the 3CN Ga sites exhibit a much higher turnover frequency than the 4CN ones. The 3CN sites are likely, therefore, to control the overall reactivity of the catalyst.

Microkinetic Modeling. Given the diversity of Ga sites in amorphous silica, the experimental evaluation of the relative contributions of different site types to the overall reaction rate and selectivity is highly nontrivial. However, such information can be readily obtained from microkinetic modeling based on DFT-derived energetics. To this end, we evaluate the kinetic parameters from the reaction free energies determined on the 3CN site, assuming that 1% of the Ga sites in the experimental loading are active. We restrict the analysis to the Ga-alkylcentered CA cycle because the DFT results strongly suggest that other cycles, with their significantly less favorable energetics, will not contribute substantially to the rate or selectivity. Further, although we have also calculated the energetics of the formation of longer Ga-C<sub>6</sub> intermediates, which competes with the  $\beta$ -hydride transfer step to liberate 1butene, we do not include these steps in the microkinetic model, as the energies conclusively show that the latter reaction is considerably more favorable (Supporting Information, S.14).

From the microkinetic analysis, we perform a degree of rate control (DRC) treatment, wherein we evaluate the sensitivity of the reaction rate to both the activation barriers of each elementary step and the binding energies of the adsorbed intermediates. The analysis is carried out with two feed compositions to illustrate the effect of different approaches to equilibrium: first, 20% ethylene (balance inert), and second, 20% ethylene, 10% 1-butene, and balance inert. In the first case, with no 1-butene in the feed, the overall conversion is 0.5%, and we find that the ethylene migratory insertion step, having a DRC of  $\sim 1$ , is rate determining. In contrast, the  $\beta$ hydride transfer step has a DRC of only  $\sim 10^{-3}$ . The most abundant surface intermediate (MASI) is ethylene physisorbed on Ga-ethyl (species 1-2, coverage of 0.99), which also has a very negative DRC value (-0.99). The Ga-n-butyl species (1-3) has a lower coverage (1%) and a less negative DRC value (-0.01). The negative DRC values for species 1-2 and 1-3are reasonable because both species block the empty sites, and a stronger binding leads to higher coverage, leaving fewer empty sites available for ethylene adsorption.

As the system comes closer to equilibrium, as is the case for the 20% ethylene/10% 1-butene feed (overall conversion of 0.3%), approximately equal coverages of *n*-butyl, species 1–3 (50%), and adsorbed ethylene, 1–2 (50%), are observed. The DRC values for the two species are –0.50. The results suggest that the TOF becomes more sensitive to the binding strength of Ga-*n*-butyl species, and this species has a higher coverage, as the reaction approaches equilibrium. At the same time,

however, the DRC value of the ethylene insertion elementary reaction remains close to 1, while the corresponding DRC value for  $\beta$ -hydride transfer remains close to zero, suggesting that there is no change in the rate determining step as the feed composition changes. The reason for the greater sensitivity to the Ga-n-butyl intermediate is, therefore, explained by the higher reverse reaction rates at higher approaches to equilibrium; the Ga-n-butyl species cannot easily cross the rate determining barrier in the reverse reaction direction, leading to greater accumulation of this species on the surface.

The above results are, finally, used to derive a simplified rate expression for oligomerization on the Ga/SiO<sub>2</sub> surface that is valid for all reaction conditions considered in this study (Supporting Information S.10). The effective activation barrier predicted by this simplified model agrees well with the barrier determined from an Arrhenius analysis of the full microkinetic model (Figure S10), further supporting the conclusions concerning the kinetically significant steps described above.

### CONCLUSIONS

A first principles study of ethylene oligomerization on amorphous silica-supported, single-site Ga<sup>3+</sup> catalysts is presented. The energetics of multiple oligomerization pathways are compared on two representative active sites, 3CN and 4CN Ga. The 4CN sites may, in principle, promote ethylene oligomerization through a proton transfer cycle, but they are not likely to be responsible for the experimentally observed reactivity due to the high ethylene insertion barrier. The 3CN Ga site, in contrast, yields a much more favorable energy landscape, which starts from a site activation process to form a Ga-alkyl species, followed by a Ga-alkyl-centered CA mechanism. With a lower activation barrier for chain termination than for ethylene insertion, the 3CN Ga sites also favor selective ethylene oligomerization to short oligomers, consistent with the experimental results at 250 °C and 1 atm. This behavior may be tied to the unusual structure of the transition state of the facile  $\beta$ -hydride transfer step, where the hydrogen being transferred does not interact directly with the Ga center. Microkinetic modeling results confirm that the ethylene insertion step is rate limiting and lead to a simplified rate expression to describe the overall kinetics. This study highlights the capability of the oxide-supported main group metals to perform olefin oligomerization chemistry and also points to principles that may facilitate the design of such catalysts, including the manipulation of the coordination environment of Ga sites to tune the catalyst reactivity.

#### ASSOCIATED CONTENT

# Supporting Information

The Supporting Information is available free of charge at https://pubs.acs.org/doi/10.1021/acscatal.1c05936.

Detailed free energy information of the analyzed reaction mechanisms, kinetic calculation details, entropy calculations, and Ga site schematics (PDF)

#### AUTHOR INFORMATION

#### **Corresponding Author**

Jeffrey Greeley — Davidson School of Chemical Engineering, Purdue University, West Lafayette, Indiana 47907, United States; orcid.org/0000-0001-8469-1715; Email: jgreeley@purdue.edu

#### **Authors**

- **Yinan Xu** Davidson School of Chemical Engineering, Purdue University, West Lafayette, Indiana 47907, United States
- Nicole J. LiBretto Davidson School of Chemical Engineering, Purdue University, West Lafayette, Indiana 47907, United States
- Guanghui Zhang Davidson School of Chemical Engineering, Purdue University, West Lafayette, Indiana 47907, United States; State Key Laboratory of Fine Chemicals, PSU-DUT Joint Center for Energy Research, School of Chemical Engineering, Dalian University of Technology, Dalian, Liaoning Province 116024, P.R. China; ocid.org/0000-0002-5854-6909
- Jeffrey T. Miller Davidson School of Chemical Engineering, Purdue University, West Lafayette, Indiana 47907, United States; orcid.org/0000-0002-6269-0620

Complete contact information is available at: https://pubs.acs.org/10.1021/acscatal.1c05936

#### **Author Contributions**

The manuscript was written through contributions of all authors. All authors have given approval to the final version of the manuscript.

#### Notes

The authors declare no competing financial interest.

# ACKNOWLEDGMENTS

This paper was based upon the work supported in part by the National Science Foundation through the Center for Innovative and Sustained Transformation of Alkane Resources (CISTAR) under Cooperative Agreement No. EEC-1647722. Use of the Center for Nanoscale Materials, an Office of Science user facility, was supported by the U.S. Department of Energy, Office of Science, Office of Basic Energy Sciences, under Contract No. DE-AC02-06CH11357. The National Energy Research Scientific Computing Center is also gratefully acknowledged. Y.X. and J.G. would like to thank Prof. Brandon C. Bukowski at Johns Hopkins University and Dr. Junnan Shangguan at UC Berkeley for insightful discussions.

## REFERENCES

- (1) Skupińska, J. Oligomerization of  $\alpha$ -Olefins to Higher Oligomers. *Chem. Rev.* **1991**, *91*, 613–648.
- (2) Yahyazadeh, A.; Dalai, A. K.; Ma, W.; Zhang, L. Fischer—Tropsch Synthesis for Light Olefins from Syngas: A Review of Catalyst Development. *Reactions* **2021**, *2*, 227–257.
- (3) Gholami, Z.; Gholami, F.; Tišler, Z.; Tomas, M.; Vakili, M. A Review on Production of Light Olefins via Fluid Catalytic Cracking. *Energies* **2021**, *14*, 1089.
- (4) Nicholas, C. P. Applications of Light Olefin Oligomerization to the Production of Fuels and Chemicals. *Appl. Catal., A* **2017**, *543*, 82–97.
- (5) McGuinness, D. S. Olefin Oligomerization via Metallacycles: Dimerization, Trimerization, Tetramerization, and Beyond. *Chem. Rev.* **2011**, *111*, 2321–2341.
- (6) Sydora, O. L. Selective Ethylene Oligomerization. *Organometallics* **2019**, *38*, 997–1010.
- (7) van Leeuwen, P. W. N. M.; Clément, N. D.; Tschan, M. J. L. New Processes for the Selective Production of 1-Octene. *Coord. Chem. Rev.* **2011**, 255, 1499–1517.
- (8) Speiser, F.; Braunstein, P.; Saussine, L. Catalytic Ethylene Dimerization and Oligomerization: Recent Developments with Nickel Complexes Containing P N-Chelating Ligands. *Acc. Chem. Res.* **2005**, 38, 784–793.

- (9) Britovsek, G. J. P.; Malinowski, R.; McGuinness, D. S.; Nobbs, J. D.; Tomov, A. K.; Wadsley, A. W.; Young, C. T. Ethylene Oligomerization beyond Schulz-Flory Distributions. *ACS Catal.* **2015**, *5*, 6922–6925.
- (10) Keim, W. Oligomerization of Ethylene to α-Olefins: Discovery and Development of the Shell Higher Olefin Process (SHOP). *Angew. Chem., Int. Ed.* **2013**, *52*, 12492–12496.
- (11) Speiser, F.; Braunstein, P.; Saussine, L. Nickel Complexes Bearing New P,N-Phosphinopyridine Ligands for the Catalytic Oligomerization of Ethylene. *Organometallics* **2004**, 23, 2633–2640.
- (12) Olivier-Bourbigou, H.; Breuil, P. A. R.; Magna, L.; Michel, T.; Espada Pastor, M. F.; Delcroix, D. Nickel Catalyzed Olefin Oligomerization and Dimerization. *Chem. Rev.* **2020**, *120*, 7919–7983.
- (13) Forget, S.; Olivier-Bourbigou, H.; Delcroix, D. Homogeneous and Heterogeneous Nickel-Catalyzed Olefin Oligomerization: Experimental Investigation for a Common Mechanistic Proposition and Catalyst Optimization. *ChemCatChem* **2017**, *9*, 2408–2417.
- (14) Martínez, A.; Arribas, M. A.; Concepción, P.; Moussa, S. New Bifunctional Ni-H-Beta Catalysts for the Heterogeneous Oligomerization of Ethylene. *Appl. Catal., A* **2013**, *467*, 509–518.
- (15) Andrei, R. D.; Popa, M. I.; Fajula, F.; Hulea, V. Heterogeneous Oligomerization of Ethylene over Highly Active and Stable Ni-AlSBA-15 Mesoporous Catalysts. *J. Catal.* **2015**, 323, 76–84.
- (16) Lin, S.; Shi, L.; Zhang, H.; Zhang, N.; Yi, X.; Zheng, A.; Li, X. Tuning the Pore Structure of Plug-Containing Al-SBA-15 by Post-Treatment and Its Selectivity for C16 Olefin in Ethylene Oligomerization. *Microporous Mesoporous Mater.* **2014**, *184*, 151–161.
- (17) Lallemand, M.; Rusu, O. A.; Dumitriu, E.; Finiels, A.; Fajula, F.; Hulea, V. NiMCM-36 and NiMCM-22 Catalysts for the Ethylene Oligomerization: Effect of Zeolite Texture and Nickel Cations/Acid Sites Ratio. *Appl. Catal., A* **2008**, 338, 37–43.
- (18) Lallemand, M.; Finiels, A.; Fajula, F.; Hulea, V. Continuous Stirred Tank Reactor for Ethylene Oligomerization Catalyzed by NiMCM-41. *Chem. Eng. J.* **2011**, *172*, 1078–1082.
- (19) Finiels, A.; Fajula, F.; Hulea, V. Nickel-Based Solid Catalysts for Ethylene Oligomerization-a Review. *Catal. Sci. Technol.* **2014**, *4*, 2412–2426.
- (20) Yeh, B.; Vicchio, S. P.; Chheda, S.; Zheng, J.; Schmid, J.; Löbbert, L.; Bermejo-Deval, R.; Gutiérrez, O. Y.; Lercher, J. A.; Lu, C. C.; Neurock, M.; Getman, R. B.; Gagliardi, L.; Bhan, A. Site Densities, Rates, and Mechanism of Stable Ni/UiO-66 Ethylene Oligomerization Catalysts. *J. Am. Chem. Soc.* **2021**, *143*, 20274–20280.
- (21) Govindasamy, A.; Markova, V. K.; Genest, A.; Rösch, N. Ethene Hydrogenation vs. Dimerization over a Faujasite-Supported [Rh(C2H4)2] Complex. A Computational Study of Mechanism. *Catal. Sci. Technol.* **2017**, *7*, 102–113.
- (22) Brogaard, R. Y.; Olsbye, U. Ethene Oligomerization in Ni-Containing Zeolites: Theoretical Discrimination of Reaction Mechanisms. ACS Catal. 2016, 6, 1205–1214.
- (23) Brogaard, R. Y.; Kømurcu, M.; Dyballa, M. M.; Botan, A.; van Speybroeck, V.; Olsbye, U.; de Wispelaere, K. Ethene Dimerization on Zeolite-Hosted Ni Ions: Reversible Mobilization of the Active Site. *ACS Catal.* **2019**, *9*, 5645–5650.
- (24) Zhou, Y.; Thirumalai, H.; Smith, S. K.; Whitmire, K. H.; Liu, J.; Frenkel, A. I.; Grabow, L. C.; Rimer, J. D. Ethylene Dehydroaromatization over Ga-ZSM-5 Catalysts: Nature and Role of Gallium Speciation. *Angew. Chem., Int. Ed.* **2020**, *59*, 19592–19601.
- (25) Pellizzeri, S.; Barona, M.; Bernales, V.; Miró, P.; Liao, P.; Gagliardi, L.; Snurr, R. Q.; Getman, R. B. Catalytic Descriptors and Electronic Properties of Single-Site Catalysts for Ethene Dimerization to 1-Butene. *Catal. Today* **2018**, *312*, 149–157.
- (26) Metzger, E. D.; Comito, R. J.; Hendon, C. H.; Dincă, M. Mechanism of Single-Site Molecule-like Catalytic Ethylene Dimerization in Ni-MFU-4l. *J. Am. Chem. Soc.* **2017**, *139*, 757–762.
- (27) LiBretto, N. J.; Xu, Y.; Quigley, A.; Edwards, E.; Nargund, R.; Vega-Vila, J. C.; Caulkins, R.; Saxena, A.; Gounder, R.; Greeley, J.; Zhang, G.; Miller, J. T. Olefin Oligomerization by Main Group Ga3+

- and Zn2+ Single Site Catalysts on SiO<sub>2</sub>. Nat. Commun. 2021, 12, 2322.
- (28) Praveen, C. S.; Borosy, A. P.; Copéret, C.; Comas-Vives, A. Strain in Silica-Supported Ga(III) Sites: Neither Too Much nor Too Little for Propane Dehydrogenation Catalytic Activity. *Inorg. Chem.* **2021**, *60*, 6865–6874.
- (29) Goldsmith, B. R.; Peters, B.; Johnson, J. K.; Gates, B. C.; Scott, S. L. Beyond Ordered Materials: Understanding Catalytic Sites on Amorphous Solids. *ACS Catal.* **2017**, *7*, 7543–7557.
- (30) Das, U.; Zhang, G.; Hu, B.; Hock, A. S.; Redfern, P. C.; Miller, J. T.; Curtiss, L. A. Effect of Siloxane Ring Strain and Cation Charge Density on the Formation of Coordinately Unsaturated Metal Sites on Silica: Insights from Density Functional Theory (DFT) Studies. ACS Catal. 2015, 5, 7177–7185.
- (31) Floryan, L.; Borosy, A. P.; Núñez-Zarur, F.; Comas-Vives, A.; Copéret, C. Strain Effect and Dual Initiation Pathway in CrIII/SiO<sub>2</sub> polymerization Catalysts from Amorphous Periodic Models. *J. Catal.* **2017**, 346, 50–56.
- (32) Fong, A.; Yuan, Y.; Ivry, S. L.; Scott, S. L.; Peters, B. Computational Kinetic Discrimination of Ethylene Polymerization Mechanisms for the Phillips (Cr/SiO<sub>2</sub>) Catalyst. *ACS Catal.* **2015**, *5*, 3360–3374.
- (33) Conley, M. P.; Delley, M. F.; Núnez-Zarur, F.; Comas-Vives, A.; Copéret, C. Heterolytic Activation of C-H Bonds on CrIII-O Surface Sites Is a Key Step in Catalytic Polymerization of Ethylene and Dehydrogenation of Propane. *Inorg. Chem.* **2015**, *54*, 5065–5078.
- (34) Roggero, I.; Civalleri, B.; Ugliengo, P. Modeling Physisorption with the ONIOM Method: The Case of NH 3 at the Isolated Hydroxyl Group of the Silica Surface. *Chem. Phys. Lett.* **2001**, *341*, 625–632.
- (35) Tielens, F.; Gierada, M.; Handzlik, J.; Calatayud, M. Characterization of Amorphous Silica Based Catalysts Using DFT Computational Methods. *Catal. Today* **2020**, *354*, 3–18.
- (36) Ugliengo, P.; Sodupe, M.; Musso, F.; Bush, I. J.; Orlando, R.; Dovesi, R. Realistic Models of Hydroxylated Amorphous Silica Surfaces and MCM- 41 Mesoporous Material Simulated by Large-Scale Periodic B3LYP Calculations. *Adv. Mater.* **2008**, *20*, 4579–4583.
- (37) Tielens, F.; Gervais, C.; Lambert, J. F.; Mauri, F.; Costa, D. Ab Initio Study of the Hydroxylated Surface of Amorphous Silica: A Representative Model. *Chem. Mater.* **2008**, *20*, 3336–3344.
- (38) Gierada, M.; Petit, I.; Handzlik, J.; Tielens, F. Hydration in Silica Based Mesoporous Materials: A DFT Model. *Phys. Chem. Chem. Phys.* **2016**, *18*, 32962–32972.
- (39) Coasne, B.; Ugliengo, P. Atomistic Model of Micelle-Templated Mesoporous Silicas: Structural, Morphological, and Adsorption Properties. *Langmuir* **2012**, *28*, 11131–11141.
- (40) Comas-Vives, A. Amorphous SiO<sub>2</sub> Surface Models: Energetics of the Dehydroxylation Process, Strain, Ab Initio Atomistic Thermodynamics and IR Spectroscopic Signatures. *Phys. Chem. Chem. Phys.* **2016**, *18*, 7475–7482.
- (41) Tuladhar, A.; Dewan, S.; Pezzotti, S.; Brigiano, F. S.; Creazzo, F.; Gaigeot, M. P.; Borguet, E. Ions Tune Interfacial Water Structure and Modulate Hydrophobic Interactions at Silica Surfaces. *J. Am. Chem. Soc.* **2020**, *142*, 6991–7000.
- (42) Ewing, C. S.; Bhavsar, S.; Veser, G.; McCarthy, J. J.; Johnson, J. K. Accurate Amorphous Silica Surface Models from First-Principles Thermodynamics of Surface Dehydroxylation. *Langmuir* **2014**, *30*, 5133–5141.
- (43) Handzlik, J.; Grybos, R.; Tielens, F. Structure of Monomeric Chromium(VI) Oxide Species Supported on Silica: Periodic and Cluster DFT Studies. *J. Phys. Chem. C* **2013**, *117*, 8138–8149.
- (44) Guesmi, H.; Gryboś, R.; Handzlik, J.; Tielens, F. Characterization of Molybdenum Monomeric Oxide Species Supported on Hydroxylated Silica: A DFT Study. *Phys. Chem. Chem. Phys.* **2014**, *16*, 18253–18260.
- (45) Guesmi, H.; Grybos, R.; Handzlik, J.; Tielens, F. Characterization of Tungsten Monomeric Oxide Species Supported on Hydroxylated Silica: A DFT Study. RSC Adv. 2016, 6, 39424–39432.

- (46) Deraet, X.; Turek, J.; Alonso, M.; Tielens, F.; Cottenier, S.; Ayers, P. W.; Weckhuysen, B. M.; de Proft, F. Reactivity of Single Transition Metal Atoms on a Hydroxylated Amorphous Silica Surface: A Periodic Conceptual DFT Investigation. *Chem. Eur. J.* **2021**, *27*, 6050–6063.
- (47) Delley, M. F.; Núñez-Zarur, F.; Conley, M. P.; Comas-Vives, A.; Siddiqi, G.; Norsic, S.; Monteil, V.; Safonova, O. V.; Copéret, C. Proton Transfers Are Key Elementary Steps in Ethylene Polymerization on Isolated Chromium(III) Silicates. *Proc. Natl. Acad. Sci. U. S. A.* 2014, 111, 11624–11629.
- (48) Kresse, G.; Furthmüller, J. Efficiency of Ab-Initio Total Energy Calculations for Metals and Semiconductors Using a Plane-Wave Basis Set. *Comput. Mater. Sci.* **1996**, *6*, 15–50.
- (49) Kresse, G.; Furthmüller, J. Efficient Iterative Schemes for Ab Initio Total-Energy Calculations Using a Plane-Wave Basis Set. *Phys. Rev. B: Condens. Matter Mater. Phys.* **1996**, *54*, 11169–11186.
- (50) Kresse, G.; Hafner, J. Ab Initio Molecular Dynamics for Liquid Metals. *Phys. Rev. B* **1993**, *47*, 558–561.
- (51) Wellendorff, J.; Lundgaard, K. T.; Møgelhøj, A.; Petzold, V.; Landis, D. D.; Nørskov, J. K.; Bligaard, T.; Jacobsen, K. W. Density Functionals for Surface Science: Exchange-Correlation Model Development with Bayesian Error Estimation. *Phys. Rev. B: Condens. Matter Mater. Phys.* **2012**, *85*, 32–34.
- (52) Joubert, D. From Ultrasoft Pseudopotentials to the Projector Augmented-Wave Method. *Phys. Rev. B: Condens. Matter Mater. Phys.* 1999, 59, 1758–1775.
- (53) Henkelman, G.; Jónsson, H. Improved Tangent Estimate in the Nudged Elastic Band Method for Finding Minimum Energy Paths and Saddle Points. *J. Chem. Phys.* **2000**, *113*, 9978–9985.
- (54) Henkelman, G.; Uberuaga, B. P.; Jónsson, H. Climbing Image Nudged Elastic Band Method for Finding Saddle Points and Minimum Energy Paths. *J. Chem. Phys.* **2000**, *113*, 9901–9904.
- (55) Smidstrup, S.; Pedersen, A.; Stokbro, K.; Jónsson, H. Improved Initial Guess for Minimum Energy Path Calculations. *J. Chem. Phys.* **2014**, *140*, 214106.
- (56) Olsen, R. A.; Kroes, G. J.; Henkelman, G.; Arnaldsson, A.; Jónsson, H. Comparison of Methods for Finding Saddle Points without Knowledge of the Final States. *J. Chem. Phys.* **2004**, *121*, 9776–9792.
- (57) Campbell, C. T. The Degree of Rate Control: A Powerful Tool for Catalysis Research. ACS Catal. 2017, 7, 2770–2779.
- (58) Schweitzer, N. M.; Hu, B.; Das, U.; Kim, H.; Greeley, J.; Curtiss, L. A.; Stair, P. C.; Miller, J. T.; Hock, A. S. Propylene Hydrogenation and Propane Dehydrogenation by a Single-Site Zn<sup>2+</sup> on Silica Catalyst. *ACS Catal.* **2014**, *4*, 1091–1098.
- (59) Novaro, O.; Chow, S.; Magnouat, P. Mechanism of Oligomerization of  $\alpha$ -Olefins with Ziegler-Natta Catalysts. *J. Catal.* **1976**, 41, 91–100.
- (60) Cavallo, L.; Guerra, G. A Density Functional and Molecular Mechanics Study of  $\beta$ -Hydrogen Transfer in Homogeneous Ziegler-Natta Catalysis. *Macromolecules* **1996**, 29, 2729–2737.